The Behavior of Electromagnetic Wave Propagation in Photonic Crystals with or without a Defect

Ayse N. Basmaci

Vocational School of Technical Sciences
Tekirdag Namik Kemal University, Tekirdag, 59030, Turkey
anbasmaci@nku.edu.tr

Abstract ─ In this study, the electromagnetic wave propagation behavior of two-dimensional photonic crystal plates with a defect is investigated. For this purpose, the partial differential equation for the electromagnetic wave propagation in various photonic crystal plates containing a defect or not is obtained by using Maxwell's equations. The defect is also defined in the electromagnetic wave propagation equation appropriately. In order to solve the electromagnetic wave propagation equation, the finite differences method is used. The material property parameters of the photonic crystal plates are determined with respect to the defects. Accordingly, the effects of material property parameters on electromagnetic wave propagation frequencies, phase velocities, and group velocities are examined. The effects of the size and position of the defects on the electromagnetic wave propagation frequencies are also discussed. The highest electromagnetic wave propagation fundamental frequency value obtained from the analyses performed is 1.198 Hz. This fundamental frequency value is obtained for the electromagnetic wave propagation in the t-shaped photonic crystal plate. Electromagnetic field distribution maps for the fundamental frequencies of the photonic crystal plates whose electromagnetic wave propagation behaviors are examined are obtained with the ANSYS package program based on the finite differences time-domain (FDTD) method.

Index Terms ─ Central finite differences method, electromagnetic wave propagation, Maxwell's equations, photonic crystals.

I. INTRODUCTION

According to the developments in optics and optoelectronics, the use of different types of materials in metamaterials, photonic crystals, and waveguides has gradually increased [1-6]. These structures are designed by combining different types of materials along a specified axis in certain ways. Phononic structures that are open to acoustic effects, in other words, affected by acoustic wave propagation, are also functionally similar to photonic structures [7-11].

Whether it is a photonic or a phononic structure, both structures consist of layers, and each layer has different material property parameters. The material property parameters include the permittivity (ε) and permeability (μ) of the structure. While analyzing the behavior of electromagnetic wave propagation in photonic structures, each layer's electromagnetic wave propagation behavior in the periodic layer group forming the structures should be considered separately. Photonic structures with a defect in some layers have also been investigated [12-14].

In the literature, there are studies that theoretically examine the electromagnetic wave propagation behavior occurring in each layer of one-dimensional and two-dimensional photonic structures [15-19], as well as experimental studies in which these structures are manufactured using various production methods [20,21]. For instance, [22-24] are among the studies investigating the electromagnetic wave propagation behavior in two-dimensional and three-dimensional plate structures.

In order to examine the electromagnetic wave propagation behavior in optical structures, many studies are guiding the formation of the partial differential equation for electromagnetic wave propagation using Maxwell's equations [25-32]. The ideal numerical method for solving the obtained partial differential equation for electromagnetic wave propagation is determined. The finite differences method is preferred in solving complex problems for which an exact solution cannot be achieved [29-33]. In [34-37], the central finite differences method is used for analyzing the electromagnetic wave propagation behavior of optical structures with microcavities, ellipses, and circular holes. The main reason for using the central finite differences method in these studies is that some nodes of the two-dimensional (2-D) structures whose electromagnetic wave propagation behaviors are investigated have different material property parameters (ε, μ) from each other.

Submitted On: February 18, 2021
Accepted On: July 7, 2021

https://doi.org/10.47037/2020.ACES.J.360603

In this study, the behaviors of electromagnetic wave propagation occurring in the two-dimensional plates with or without a defect are investigated. The effects of the location and size of the defect in the plates on the electromagnetic wave propagation frequencies are also examined. For this purpose, the material property parameters (ε, μ) of the defects are determined as zero. Accordingly, the frequencies of electromagnetic wave propagation in the plate with the defect are obtained using the central finite differences method. In addition, phase velocities and group velocities of the electromagnetic wave propagation are examined. The electromagnetic field distribution maps for the fundamental frequencies of the photonic crystal plates are visualized by using the ANSYS Lumerical package program. The novelty of this study is that it describes the effects of the defect locations and defect sizes of the 2-D photonic crystal plates formed in different shapes on frequencies of the electromagnetic wave propagation in the photonic crystal plates.

II. THEORETICAL ANALYSIS

The partial differential equation for the electromagnetic wave (EMW) propagation occurring in the two-dimensional plate is obtained using Maxwell's equations. The finite difference method is preferred in the solution of the electromagnetic wave propagation equation to examine the behavior of electromagnetic wave propagation in two-dimensional plates which have a defect or which have not. A two-dimensional plate positioned in the Cartesian coordinate system can be seen in Fig. 1.

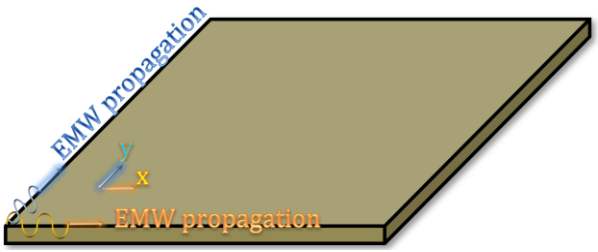

Fig. 1. A view of a 2-D plate.

In a source free, linear, isotropic and homogenous region, The first-order Maxwell's curl equations are as follows [38]:

$$\nabla \cdot \vec{E} = \frac{\rho}{\varepsilon}, \quad (1a)$$

$$\nabla \cdot \vec{H} = 0, \quad (1b)$$

$$\nabla \times \vec{E} = -i\omega\mu\vec{H}, \quad (1c)$$

$$\nabla \times \vec{H} = -i\omega\varepsilon\vec{E}, \quad (1d)$$

where $i{:}\sqrt{-1}$, ρ is the charge density, μ is the permeability, ε is the permittivity, E is the electrical field, and H is the magnetic field.

Using Eqs. (1c) and (1d), Eq. (2) is obtained as in the following form:

$$\nabla \times \left(\nabla \times \vec{H}\right) = \nabla\left(\nabla \cdot \vec{H}\right) - \nabla^2\vec{H} = \nabla \times \left(-\mu\frac{\partial \vec{H}}{\partial t}\right), \quad (2)$$

where $H(x,y,t)$ represents the electromagnetic wave propagation field of the 2-D plate. Partial differential equation with respect to time and position related to electromagnetic wave propagation obtained by solution of Eq. (2) is as follows:

$$\frac{\partial^2 H(x,y,t)}{\partial x^2} + \frac{\partial^2 H(x,y,t)}{\partial y^2} - \mu\varepsilon\frac{\partial^2 H(x,y,t)}{\partial t^2} = 0. \quad (3)$$

D_x represents the material property parameters of (μ_x ε_x) on the x-axis, and D_y represents the material property parameters of (μ_y ε_y) on the y-axis. Accordingly, Eq. (3) is rearranged as follows:

$$D_x\frac{\partial^2 H(x,y,t)}{\partial x^2} + D_y\frac{\partial^2 H(x,y,t)}{\partial y^2} - \frac{\partial^2 H(x,y,t)}{\partial t^2} = 0. \quad (4)$$

Solving Eq. (4) for D_x=D_y=1 and $H(x,y,t) = he^{-i(-\beta_m x - \beta_n y + \omega t)}$ for the linear isotropic case, Eq. (5) is obtained as follows:

$$\beta_m{}^2 + \beta_n{}^2 - \omega_{mn}{}^2 = 0, \quad (5a)$$

$$\beta_m{:}\frac{m\pi}{a},\ \beta_n{:}\frac{n\pi}{b}\ \ and\ \ m{:}\,0,1,2\ldots,\ n{:}\,0,1,2\ldots, \quad (5b)$$

$$\omega_{mn} = \sqrt{\left(\frac{m\pi}{a}\right)^2 + \left(\frac{n\pi}{b}\right)^2}, \quad (5c)$$

where h, β_m, β_n, ω_{mn}, represents travelling wave, wave number for the x-axis, wave number for the y-axis and electromagnetic wave propagation frequency, respectively. In this study, the permittivity (ε) and permeability (μ) values of the plate are assumed as 1 for the defect-free parts of the plate. In keeping with this assumption, there are some studies on silicon-based photonic metamaterials in the literature [40,41]. The b/a ratio of the 2-D plate is considered in units, where a represents the plate's width and b represents the plate's length, and its value is considered as 1/1. The exact solution of Eq. (4) given in Eqs. (5a-5c) is obtained when the material property parameters D_x and D_y are equal to 1. In the fundamental mode, where the value of the (m, n) mode pair is equal to (1,1), the value of ω_{11} from the exact solution of Eq. (4) is obtained as 4.442 Hz. Especially in the analysis of the electromagnetic wave propagation behavior occurring in the plate with a defect, the central finite differences method should be used to solve Eq. (4). Accordingly, to apply the finite differences method, the 2-D plate is expressed with nodes, as shown in Fig. 2. Besides, the representation of any node is represented by (k,l), while Δ represents the neighborhoods with respect to the specified (k,l) node.

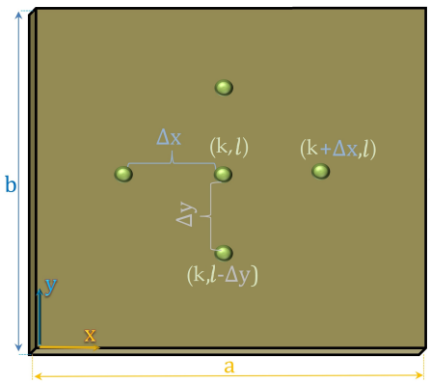

Fig. 2. Central finite differences notation of the plate.

According to the derivative values obtained using the Taylor series expansion and given in Table 1, the central finite differences method is applied to Eq. (4).

Table 1: The central finite differences notation [39]

Derivative	**The Central Finite Differences Notation O(h²)**
$h(x,y)$	$\approx\ q_{k,l}$
$\frac{\partial^2 h(x,y)}{\partial x^2}$	$\approx \frac{q_{k-1,l} - 2q_{k,l} + q_{k+1,l}}{\Delta x^2}$
$\frac{\partial^2 h(x,y)}{\partial y^2}$	$\approx \frac{q_{k,l-1} - 2q_{k,l} + q_{k,l+1}}{\Delta y^2}$

By defining the neighbours of the *(k,l)* node with the Taylor Series expansion, the expression obtained is as follows:

$$q_{k\pm1,l} = q_{k,l} \pm \frac{\Delta x}{1!}\frac{\partial q}{\partial x} + \frac{\Delta x^2}{2!}\frac{\partial^2 q}{\partial x^2} \pm \mathrm{R}, \quad (6a)$$

$$q_{k,l\pm1} = q_{k,l} \pm \frac{\Delta y}{1!}\frac{\partial q}{\partial y} + \frac{\Delta y^2}{2!}\frac{\partial^2 q}{\partial y^2} \pm \mathrm{R}, \quad (6b)$$

where R represents truncation. The order of the truncation here is $O(h^2)$ since it comes after the second-order derivative.

Applying $H(x,y,t) = h(x,y)e^{-i\omega t}$ transformation to Eq. (4), Eq. (7a) is obtained. Equation (7a) is rearranged according to the values given in Table 1 by the method of central finite differences and thus Eq. (7b) is obtained. Relevant equations are as the following forms:

$$D_x\left[\frac{\partial^2 h(x,y)}{\partial x^2}\right] + D_y\left[\frac{\partial^2 h(x,y)}{\partial y^2}\right] + \omega^2 h(x,y) = 0, \quad (7a)$$

$$D_x\left[\frac{q_{k-1,l}-2q_{k,l}+q_{k+1,l}}{\Delta x^2}\right] + D_y\left[\frac{q_{k,l-1}-2q_{k,l}+q_{k,l+1}}{\Delta y^2}\right] + \omega^2 q_{k,l} = 0. \quad (7b)$$

Boundary conditions need to be determined to solve Eq. (7b). There is no electromagnetic interaction in the frame parts of the 2-D plate, which is seen in Fig. 4 and consists of 4 nodes. The nodes of this plate that interact with each other are (1,1), (2,1), (1,2), and *(k,l)*, respectively. Using these nodes, an eigenvector *M(ω)* is obtained to determine the frequency values by solving Eq. (7b). For the plate with four nodes starting from the node (1,1) to (2,2), the eigenvector *M(ω)* obtained by arranging Eq. (7b) according to the values *k:2* and *l:2* is as follows:

$$M(\omega) = \left[\begin{bmatrix} p(\omega) & s & z & 0 \\ s & p(\omega) & z & 0 \\ z & 0 & p(\omega) & s \\ 0 & z & s & p(\omega) \end{bmatrix}\right]_{k\times l} = 0. \quad (8)$$

The terms in Eq. 8 are defined as follows:

$$p(\omega) = -2\left(\frac{D_x}{\Delta x^2} + \frac{D_y}{\Delta y^2} + \omega^2\right), \quad (9a)$$

$$s = \frac{D_x}{\Delta x^2}, \quad (9b)$$

$$z = \frac{D_y}{\Delta y^2}. \quad (9c)$$

For the plate with four nodes, the distance for each adjacent node is defined as $\Delta x = \Delta y = \frac{1}{3}$.

The steps of the theoretical analysis are summarized in the flowchart, as also seen from Fig. 3.

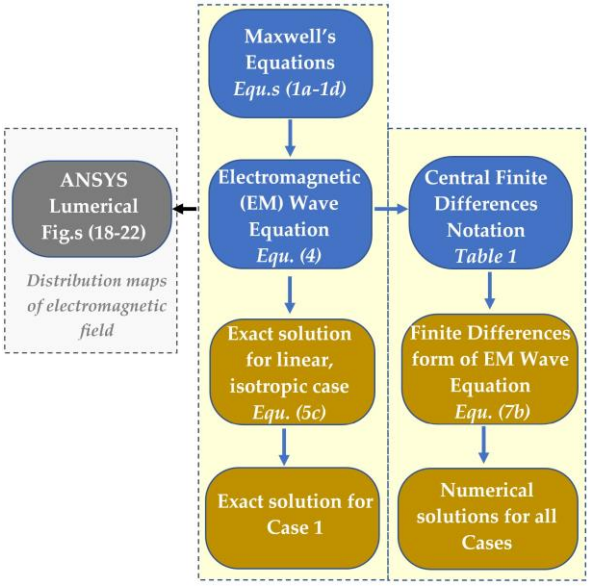

Fig. 3. The flowchart summarizing the theoretical analysis.

Electromagnetic wave propagation frequencies, in other words, ω_{mn} eigenvalues, are obtained by equating the determinant of the eigenvector *M(ω)* to zero.

Besides, the phase velocities, v_{phase} and group velocities, v_{group} regarding the electromagnetic wave propagation occurring in the plate are calculated with the following formulas:

$$v_{phase} = \frac{\omega_{mn}}{\beta_n}, \quad (10a)$$

$$v_{group} = \frac{\partial \omega_{mn}}{\partial \beta_n}. \quad (10b)$$

The behaviour of electromagnetic wave propagation occurring in a two-dimensional plate can be defined using Eqs. (7b) and (8). Accordingly, electromagnetic wave propagation frequencies are obtained for six different cases where the plate has a defect from various parts, whether it has not. Figure 4 shows the first case (Case 1) where the plate has not any defect.

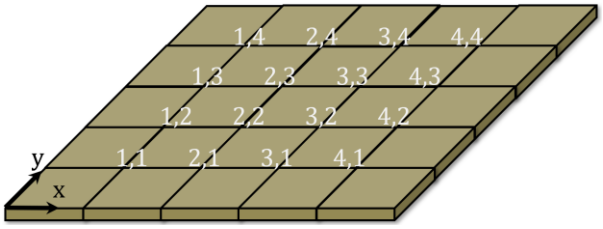

Fig. 4. A plate which has not any defect – Case 1.

In all other cases except the first case, plates have a defect in their various parts. Figure 5 shows the second case (Case 2), where the plate has an unsymmetrical O-shaped defect. In this case, there are two nodes with a defect. Nodes with the defect are (3,2) and (3,3) nodes, respectively.

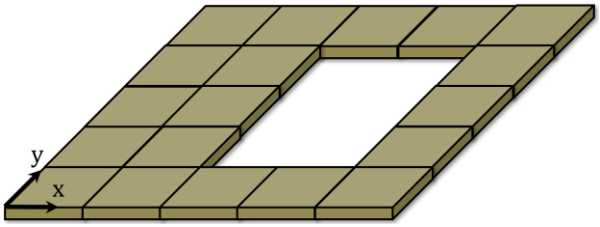

Fig. 5. A plate with an unsymmetrical O-shaped defect – Case 2.

Figure 6 shows the third case (Case 3), where the plate has a symmetrical O-shaped defect. In this case, there are four nodes with a defect. Nodes with the defect are (2,2), (2,3), (3,2) and (3,3) nodes, respectively.

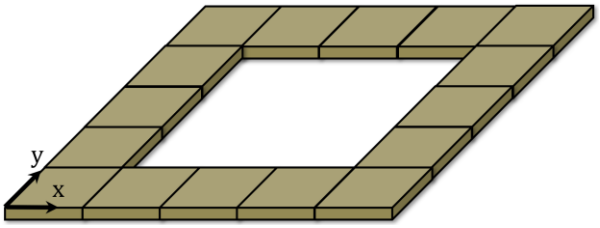

Fig. 6. A plate with a symmetrical O-shaped defect – Case 3.

Figure 7 shows the fourth case (Case 4), where the plate has an unsymmetrical C-shaped defect. In this case, there are four nodes with a defect. Nodes with the defect are (3,2), (3,3), (4,2) and (4,3) nodes, respectively.

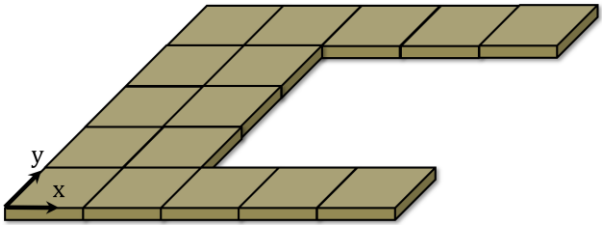

Fig. 7. A plate with a C-shaped defect – Case 4.

Figure 8 shows the fifth case (Case 5), where the plate has a L-shaped defect. In this case, there are four nodes with a defect. Nodes with the defect are (3,3), (4,3), (3,4) and (4,4) nodes, respectively.

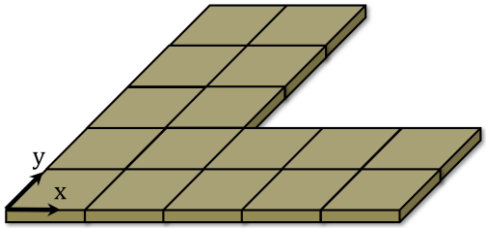

Fig. 8. A plate with a L-shaped defect – Case 5.

Figure 9 shows the sixth case (Case 6), where the plate has a symmetrical t-shape and corner defects. In this case, there are four nodes with a defect. Nodes with the defect are (1,1), (1,4), (4,1) and (4,4) nodes, respectively.

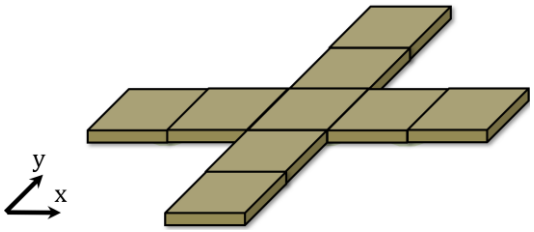

Fig. 9. A t-shaped plate with corner defects– Case 6.

The frequencies of the electromagnetic wave propagation occurring in the 2-D plate, which has the defect in its various regions, are analyzed using the method of central finite differences for multiple cases, defined according to the nodes where the defect has been placed in the plate. In this analysis made with the method of central finite differences, the material property parameters (ε, μ) of the nodes with the defect are defined as zero.

III. RESULTS AND DISCUSSIONS

The frequencies related to the electromagnetic wave propagation occurring in the defect-free plate defined as Case 1 are examined for various (m, n) modes. This analysis is carried out using both the exact solution and the finite differences method. As shown in Fig. 10 and Fig. 11, the electromagnetic wave propagation frequencies obtained from the exact solution are relatively close to the values of the frequencies obtained by the finite difference method. Additionally, Fig. 10 shows that the frequencies of electromagnetic wave propagation increase linearly as the wavenumber increases.

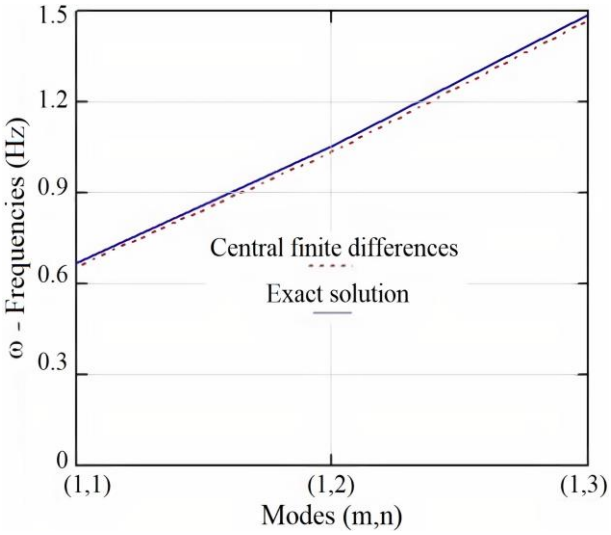

Fig. 10. Dispersion relation (β-ω) of the electromagnetic wave for Case 1.

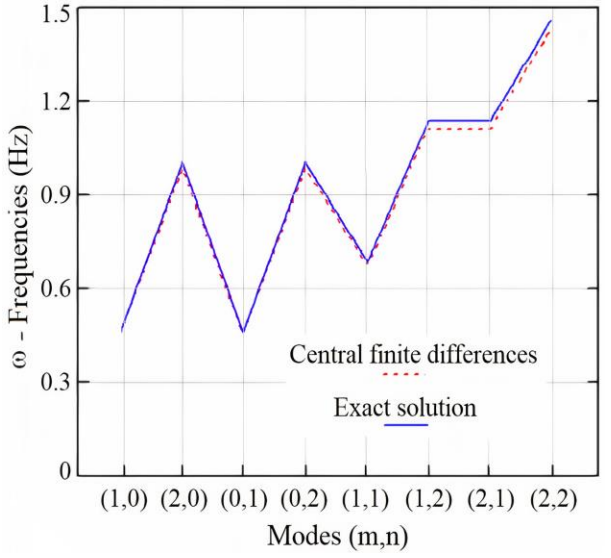

Fig. 11. Comparison of the frequencies obtained by the exact solution and finite differences method for Case 1.

Table 2: The frequency investigation of five different cases (Cases 2-6) of the plate

	Case No	Mode – (m,n)	Frequency (Hz)
DEFECT-FREE	1	(1,0)	0.492
		(2,0)	0.984
		(0,1)	0.492
		(0,2)	0.984
		(1,1) - Fundamental Mode for 2-D Plate	0.696
		(1,2)	1.100
		(2,1)	1.100
		(2,2)	1.391
INTERNAL DEFECTED	2	(1,0)	0.492
		(2,0)	0.984
		(0,1)	0.492
		(0,2)	0.984
		(1,1)	0.911
		(1,2)	1.260
		(2,1)	1.428
		(2,2)	1.821
	3	(1,0)	0.492
		(2,0)	0.984
		(0,1)	0.492
		(0,2)	0.984
		(1,1)	1.125
		(1,2)	1.485
		(2,1)	1.485
		(2,2)	2.251
	4	(1,0)	0.492
		(2,0)	0.984
		(0,1)	0.492
		(0,2)	0.984
		(1,1)	0.912
		(1,2)	1.260
		(2,1)	1.432
		(2,2)	1.824
CORNER DEFECTED	5	(1,0)	0.492
		(2,0)	0.984
		(0,1)	0.492
		(0,2)	0.984
		(1,1)	0.846
		(1,2)	1.245
		(2,1)	1.245
		(2,2)	1.695
	6	(1,0)	0.492
		(2,0)	0.984
		(0,1)	0.492
		(0,2)	0.984
		(1,1)	1.198
		(1,2)	2.009
		(2,1)	2.009
		(2,2)	2.397

In this study, plates can be grouped into three different classes in terms of the shape of the defects they have. These classes include plates without defects, plates with internal defects, and plates with corner defects, respectively. Case 1 represents the class of plates without defects. Case 2, Case 3, and Case 4 represent the class of plates with internal defects. Case 5 and Case 6 represent the class of plates with corner defects. As can be seen from Table 2, the frequency values of electromagnetic wave propagation occurring in the plates for all these cases are calculated in the lower modes with the finite differences method.

Figure 12 depicts the dispersion relation of the electromagnetic wave for all cases. Among these six cases, the lowest electromagnetic wave propagation frequencies are obtained for Case 1, while the highest wave propagation frequencies are obtained for Case 6. In addition, the second highest electromagnetic wave propagation frequencies are obtained for Case 3.

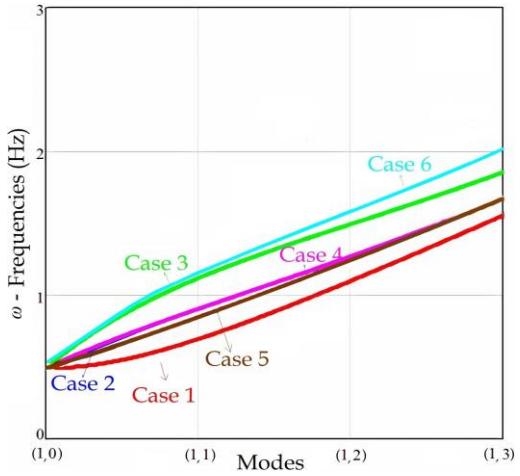

Fig. 12. Dispersion relation of the electromagnetic wave in the lower modes for all cases.

Figure 13 shows the dispersion relation of the electromagnetic wave in the higher modes. In Fig. 12, curves related to the dispersion relation of the electromagnetic wave obtained for Case 2 and Case 4 in the lower modes are almost coincident, whereas, in Fig. 13, the difference between these curves can be clearly seen in the higher modes. The frequencies of electromagnetic wave propagation obtained for Case 2, Case 3, and Case 4 reach a peak value and then their values decrease to zero. It should also be noted that the frequency values of the electromagnetic wave propagation obtained for Case 2, Case 3, and Case 4 decrease towards zero in (1.27), (1.23), and (1.28) modes, respectively. The electromagnetic wave propagation frequency values obtained for Case 1 increase linearly with the increase in the mode values, whereas the electromagnetic wave propagation frequency values obtained for Case 5 and Case 6 increase exponentially.

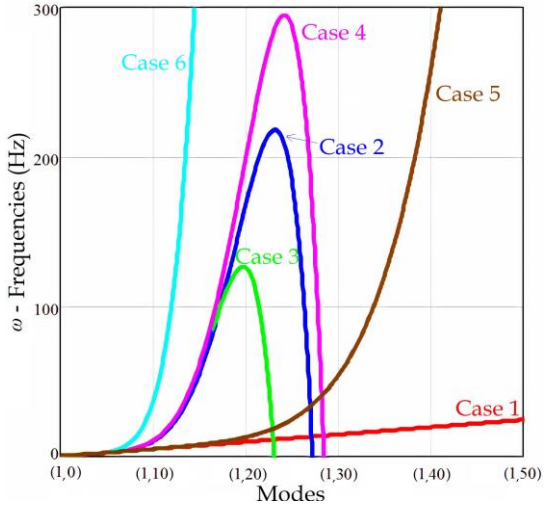

Fig. 13. Dispersion relation of the electromagnetic wave in the higher modes for all cases.

The phase and group velocity values in Figs. 14-17 are obtained by means of Eqs. (10a) and (10b). Figure 14 shows the phase velocity values obtained in the lower modes. All phase velocity values obtained in the lower modes decrease with the increase of the mode values. It should be noted that the highest phase velocity value is obtained for Case 6, whereas the lowest phase velocity value is obtained for Case 1.

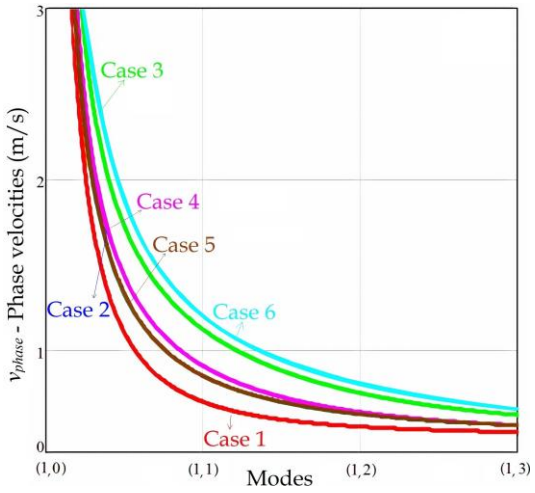

Fig. 14. Phase velocities in the lower modes for all cases.

As can be seen from Fig. 15, values of the phase velocities obtained for Case 2, Case 3, and Case 4 in the higher modes decrease towards zero after reaching a certain peak. The peak values of the phase velocities obtained for Case 2, Case 3, and Case 4 are 9.6 m/s,

6.5 m/s, and 12.4 m/s, respectively.

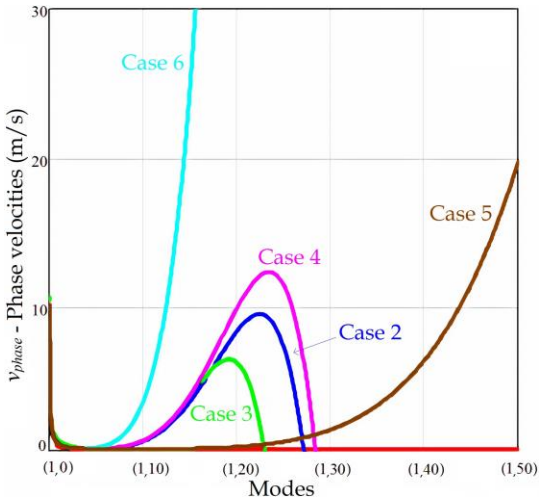

Fig. 15. Phase velocities in the higher modes for all cases.

Figure 16 depicts the group velocities in the lower modes for all cases. In the lowest modes, while the mode value increases from (1.0) to (1.1), the group velocities obtained for Case 3 and Case 6 decrease negatively exponentially, the group velocities obtained for Case 2 and Case 4 decrease linearly, the group velocities obtained for Case 5 increase linearly at the low slope, and the group velocities obtained for Case 1 increase logarithmically. In addition, in all other modes greater than (1.1), the group velocities increase with the increase of the modes for all cases.

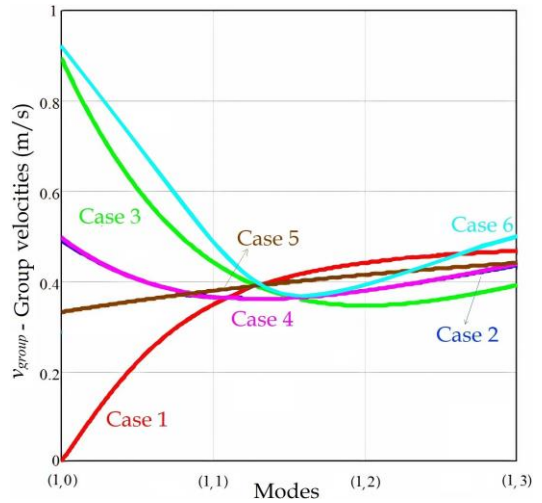

Fig. 16. Group velocities in the lower modes for all cases.

As shown in Fig. 17, the values of the group velocities obtained for Case 2, Case 3, and Case 4 in the higher modes decrease towards zero after reaching a certain peak. Peak values of the group velocities obtained for Case 2, Case 3, and Case 4 are 33.1 m/s, 17.9 m/s, and 25.6 m/s, respectively.

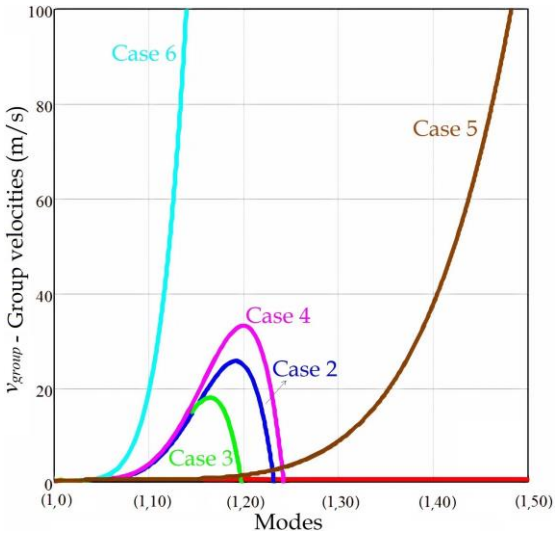

Fig. 17. Group velocities in the higher modes for all cases.

In Figs. 18-22, electromagnetic field distribution and material property parameters (ε, μ) distribution maps of five different cases (Cases 2-6) of the plate with the defect are depicted. The electromagnetic field and material property parameters (ε, μ) distribution maps in the (1,1) mode, the fundamental frequency mode for 2-D plates, are obtained using the ANSYS package program based on finite differences time-domain method. It should be noted that the data obtained from electromagnetic field distribution maps show a very good agreement with the data obtained from material property parameters (ε, μ) distribution maps.

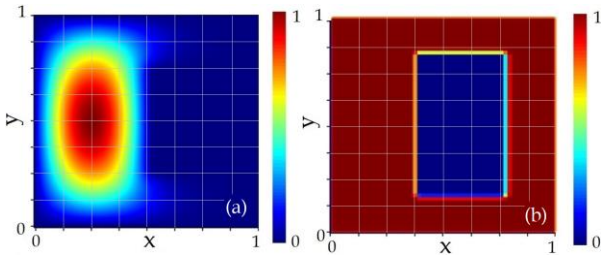

Fig. 18. Distribution maps of (a) electromagnetic field, and (b) material property parameters (ε, μ) for Case 2.

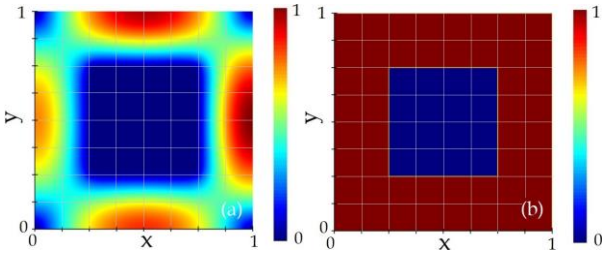

Fig. 19. Distribution maps of (a) electromagnetic field, and (b) material property parameters (ε, μ) for Case 3.

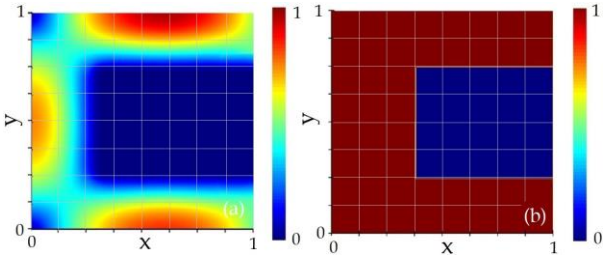

Fig. 20. Distribution maps of (a) electromagnetic field, and (b) material property parameters (ε, μ) for Case 4.

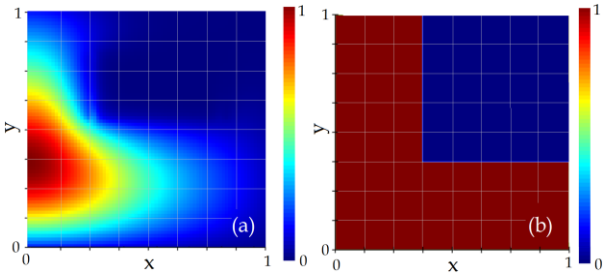

Fig. 21. Distribution maps of (a) electromagnetic field, and (b) material property parameters (ε, μ) for Case 5.

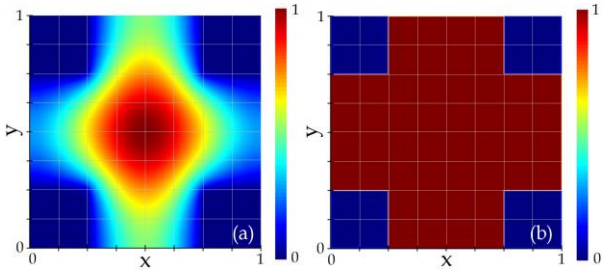

Fig. 22. Distribution maps of (a) electromagnetic field, and (b) material property parameters (ε, μ) for Case 6.

VI. CONCLUSION

In this study, the behaviors of electromagnetic wave propagation occurring in the two-dimensional plates having defects in their different parts are investigated. The behavior of electromagnetic wave propagation in the two-dimensional plate which has not any defect is also examined. For this purpose, the electromagnetic wave propagation frequencies are obtained in the fundamental mode for a total of six different cases, including the five different cases of defects in different parts of the plate and the condition of being defect-free. For the five cases where the plate has a defect, the effects of the defect's region and its size on the fundamental frequencies of electromagnetic wave propagation are discussed. The electromagnetic wave propagation frequencies obtained for six different cases are compared. As the material property parameters (ε, μ) of some nodes on the plate take zero value, in other words, with the increase in the size of the defected part of the plate, the obtained electromagnetic wave propagation frequency values also increase. The highest electromagnetic wave propagation frequency values are obtained for the corner-defected, t-shaped plate, while the electromagnetic wave propagation frequency values obtained for the O-shaped plate are second in the ranking. When the frequencies of the electromagnetic wave propagation are examined in the higher modes, it also allows making comments about the characteristics of the phase and group velocities. In the higher modes, the frequency values of the electromagnetic wave propagation occurring in the internal-defected plates become zero after a certain mode value. In addition, the increase in the frequencies of the electromagnetic wave propagation that occur in the corner-defected plates in the higher modes is exponential and continuous with the increase in the mode values. The lowest electromagnetic wave propagation frequency values are obtained when the plate does not have a defect. The electromagnetic wave propagation frequencies obtained in this case increase linearly with the increase in the mode values.

In this study, the preferred numerical solution method is the central finite differences method. Choosing the central finite differences method as the solution method enables adjusting the material properties parameters of any point of the structure whose electromagnetic wave propagation frequencies are examined. Thus, the electromagnetic wave propagation behavior for any complex structure can be easily determined.

In future studies, it is also possible to apply the analysis to three-dimensional structures and determine the acoustic wave propagation behavior in complex phononic structures by taking advantage of the central finite differences method.

REFERENCES

[1] K. H. Chung, T. Kato, S. Mito, H. Takagi, and M. Inoue, "Fabrication and characteristics of one-dimensional magnetophotonic crystals for magneto-optic spatial light phase modulators," *Journal of Applied Physics*, vol. 107, pp. 09A930, Apr. 2010.

[2] E. A. Kadomina, E. A. Bezus, and L. L. Doskolovich, "Generation of interference patterns of evanescent electromagnetic waves at Fabry-

Perot resonances of 1D photonic crystal modes," in *3rd. International Conference "Information Technology and Nanotechnology," (ITNT-2017)*, Samara, pp. 42-47, 2017.

[3] A. M. Singer, A. M. Heikal, H. El-Mikati, S. S. A. Obayya, and M. F. O. Hameed, "Ultra-low loss and flat dispersion circular porous core photonic crystal fiber for terahertz waveguiding," *Applied Computational Electromagnetics Society Journal*, vol. 35, no. 6, pp. 709-717, June 2020.

[4] Y. Zhang, Z. Cao, G. Lu, D. Zeng, M. Li, and R. Wang, "Reconfigurable array designed for directional EM propagation using energy band theory of photonic crytals," *Applied Computational Electromagnetics Society Journal*, vol. 33, no. 11, pp. 1209-1216, Nov. 2018.

[5] S. Jahani and Z. Jacob, "All-dielectric metamaterials," *Nature Nanotechnology*, vol. 11, pp. 23-36, Jan. 2016.

[6] S.-Y. Sung, A. Sharma, A. Block, K. Keuhn, and B. J. H. Stadler, "Magneto-optical garnet waveguides on semiconductor platforms: Magnetics, mechanics, and photonics," *Journal of Applied Physics*, vol. 109, pp. 07B738, Mar. 2011.

[7] H. Sun, S. Huang, Q. Wang, S. Wang, and W. Zhao, "Improvement of unidirectional focusing periodic permanent magnet shear-horizontal wave electromagnetic acoustic transducer by oblique bias magnetic field," *Sensors and Actuators A: Physical*, vol. 290, pp. 36-47, May 2019.

[8] A. Ayman, S. Prasad, and V. Singh, "Tuning the band structures and electromagnetic density of modes in fused Silica slab by acoustic waves," *Optik – International Journal for Light and Electron Optics*, vol. 204, 164105, Feb. 2020.

[9] A. Rostami, H. Kaatuzian, and B. Rostami-Dogolsara, "Acoustic 1 x 2 demultiplexer based on fluid-fluid phononic crystal ring resonators," *Journal of Molecular Liquids*, vol. 308, 113144, Apr. 2020.

[10] A. Rostami, H. Kaatuzian, and B. Rostami-Dogolsara, "Design and analysis of tunable acoustic channel drop filter based on fluid-fluid phononic crystal ring resonators," *Wave Motion*, vol. 101, 102700, Mar. 2021.

[11] A. Trzaskowska, P. Hakonen, M. Wiesner,, and S. Mielcarek, "Generation of a mode in phononic crystal based on 1D/2D structures," *Ultrasonics*, vol. 106, 106146, Aug. 2020.

[12] A. Madani and S. R. Entezar, "Tunable enhanced Goos-Hanchen shift in one-dimensional photonic crystals containing graphene monolayers," *Superlattices and Microstructures*, vol. 86, pp. 105-110, Oct. 2015.

[13] A. Aghajamali, T. Alamfard, and C. Nayak, "Investigation of reflectance properties in a symmetric defective annular semiconductor-superconductor photonic crystal with a radial defect layer," *Physica B: Physics of Condensed Matter*, 412770, Mar. 2021.

[14] T. Jalali, A. Gharaati, and M. Rastegar, "Enhanced of Faraday rotation in defect modes of one-dimensional magnetophotonic crystals," *Materials Science-Poland*, vol. 37, no. 3, pp. 446-453, Oct. 2019.

[15] O. V. Shramkova and Y. A. Olkhovskiy, "Electromagnetic wave transmission and reflection by a quasi-periodic layered semiconductor structure," *Physica B: Physics of Condensed Matter*, vol. 406, no. 8, pp. 1415-1419, Apr. 2011.

[16] A. N. Basmaci, "Characteristics of electromagnetic wave propagation in a segmented photonic waveguide," *Journal of Optoelectronics and Advanced Materials*, vol. 22, no. 9-10, pp. 452-460, Sep.-Oct. 2020.

[17] H. Wang, Y. Chen, and C. Huang, "The electromagnetic waves propagation characteristics of inhomogeneous dusty plasma," *Optik – International Journal for Light and Electron Optics*, vol. 196, 163148, Nov. 2019.

[18] F. Meng, L. Du, A. Yang, and X. Yuan, "Low loss surface electromagnetic waves on a metal-dielectric waveguide working at short wavelength and aqueous environment," *Optics Communications*, vol. 433, pp. 10-13, Feb. 2019.

[19] A. B. Khanikaev, S. H. Mousavi, C. Wu, N. Dabidian, K. B. Alici, and G. Shvets, "Electromagnetically induced polarization conversion," *Optics Communications*, vol. 285, pp. 3423-3427, July 2012.

[20] M. Askari, D. Hutchins, P. J. Thomas, L. Astolfi, R. L. Watson, M. Abdi, M. Ricci, S. Laureti, L. Nie, S. Freear, R. Wildman, C. Tuck, M. Clarke, E. Woods, and A. T. Clare, "Additive manufacturing of metamaterials: A review," *Additive Manufacturing*, vol. 36, 101562, Dec. 2020.

[21] K. Bi, Q. Wang, J. Xu, L. Chen, C. Lan, and M. Lei, "All-dielectric metamaterial fabrication techniques," *Advanced Optical Materials*, vol. 9, 2001474, Nov. 2021.

[22] T. Gao, H. Sun, Y. Hong, and X. Qing, "Hidden corrosion detection using laser ultrasonic guided waves with multi-frequency local wavenumber estimation," *Ultrasonics*, vol. 108, 106182, Dec. 2020.

[23] T. F. Khalkhali and A. Bananej, "Effect of shape of scatterers and plasma frequency on the complete photonic band gap properties of two-dimensional dielectric-plasma photonic crystals," *Physics Letters A*, vol. 380, pp. 4092-4099, Dec. 2016.

[24] B. Zamir, R. Ali, and M. Bashir, "Electromagnetic wave propagation in a superconducting parallel-

plate waveguide filled with an indefinite medium," *Results in Physics*, vol. 13, 102312, June 2019.
[25] K. S. Kunz and R. J. Luebbers, *The Finite Difference Time Domain Method for Electromagnetics*. CRC Press, London, 1993.
[26] S. Caorsi and G. Cevini, "Assessment of the performances of first- and second-order time-domain ABC's for the truncation of finite element grids," *Microwave Optical Technology Letters*, vol. 38, no. 1, pp. 11-16, May 2003.
[27] J. Li and Z. Zhang, "Unified analysis of time domain mixed finite element methods for Maxwell's equations in dispersive media," *Journal of Computational Mathematics*, vol. 28, no. 5, pp. 693-710, Sep. 2010.
[28] L. Li, B. Wei, Q. Yang, and D. Ge, "Piecewise linear recursive convolution finite element time domain method for electromagnetic analysis of dispersive media," *Optik – International Journal for Light and Electron Optics*, vol. 198, 163196, Dec. 2019.
[29] S. Elshahat, I. Abood, Z. Liang, J. Pei, and Z. Ouyang, "Dispersive engineering of W2 steeple-house-defect waveguide photonic crystals," *Results in Physics*, vol. 19, 103547, Dec. 2020.
[30] J.-Y. Lee, J.-H. Lee, and H.-K. Jung, "Linear lumped loads in the FDTD method using piecewise linear recursive convolution method," *IEEE Microwave and Wireless Componenets Letters*, vol. 16, no. 4, Apr. 2006.
[31] S. S. Neoh and F. Ismail, "Time-explicit numerical methods for Maxwell's equation in second-order form," *Applied Mathematics and Computation*, vol. 392, 125669, Mar. 2021.
[32] X. Jia, Q. Meng, X. Wang, and Z. Zhou, "Numerical study of a quasi-zero-index photonic metamaterials," *Optics Communications*, vol. 364, pp. 158-164, Apr. 2016.
[33] F. Kaburcuk and A. Z. Elsherbeni, "A speeding up technique for lossy anisotropic algorithm in FDTD method," *Applied Computational Electromagnetics Society Journal*, vol. 31, no. 12, pp. 1377-1381, Dec. 2016.
[34] B. Meng, L. Wang, W. Huang, X. Li, X. Zhai, and H. Zhang, "Wideband and low dispersion slow-light waveguide based on a photonic crystal with crescent-shaped air holes," *Applied Optics*, vol. 51, no. 23, pp. 5735-5742, Aug. 2012.
[35] C. Shi, J. Yuan, X. Luo, S. Shi, S. Lu, P. Yuan, W. Xu, Z. Chen, and H. Yu, "Transmission characteristics of multi-structure bandgap for lithium niobate integrated photonic crystal and waveguide," *Optics Communications*, vol. 461, 125222, Apr. 2020.
[36] C. Shi, J. Yuan, X. Luo, S. Shi, S. Lu, P. Yuan, W. Xu, Z. Chen, and H. Yu, "Multi-channel slow light coupled-resonant waveguides based on photonic crystal with rectangular microcavities," *Optics Communications*, vol. 341, pp. 257-262, Apr. 2015.
[37] V. Varmazyari, H. Habibiyan, and H. Ghafoorifard, "Slow light in ellipse-hole photonic crystal line-defect waveguide with high normalized delay bandwidth product," *Journal of the Optical Society of America B*, vol. 31, pp. 771-779, Mar. 2014.
[38] D. M. Pozar, *Microwave Engineering*. 4th Edition, John Wiley & Sons, Inc., Amherst, Massachusetts, 2012.
[39] J. H. Mathews and K. D. Fink, *Numerical Methods using Matlab*. Prince Hall, New Jersey, 1999.
[40] M. Moitra, B. A. Slovick, Z. G. Yu, S. Krishnamurthy, and J. Valentine, "Experimental demonstration of a broadband all-dielectric metamaterial perfect reflector," *Applied Physics Letters*, vol. 104, 171102, Apr. 2014.
[41] J. C. Ginn and I. Brener, "Realizing optical magnetism from dielectric metamaterials," *Physical Review Letters*, vol. 108, 097402, Feb. 2012.

Ayse Nihan Basmaci received her B.Sc., M.Sc. and Ph.D. degrees in Electrical Electronics Engineering from Pamukkale University in 2008, 2011 and 2017, respectively. Between 2008 and 2012, she worked as an Engineer at Turk Telekom Company. She also has been an Assistant Professor at Tekirdag Namik Kemal University, Vocational School of Technical Sciences, in the last 2 years. Her research interests include electromagnetic wave propagation, photonics, advanced materials, computational electromagnetics, electro-magnetic fields, electromagnetic waves, and microwave filter design.